

# Flat-band Fulde–Ferrell–Larkin–Ovchinnikov State from Quantum Geometry Discrepancy

Zi-Ting Sun,<sup>1,\*</sup> Ruo-Peng Yu,<sup>1,\*</sup> Shuai A. Chen,<sup>1</sup> Jin-Xin Hu,<sup>1,2,†</sup> and K. T. Law<sup>1,‡</sup>

<sup>1</sup>*Department of Physics, Hong Kong University of Science and Technology, Clear Water Bay, Hong Kong, China*

<sup>2</sup>*Division of Physics and Applied Physics, School of Physical and Mathematical Sciences, Nanyang Technological University, Singapore 637371*

(Dated: August 2, 2024)

The Fulde–Ferrell–Larkin–Ovchinnikov (FFLO) state, a finite-momentum superconducting pairing state, has been extensively studied from the perspective of mismatched Fermi surfaces of paired electrons. In this work, we propose a distinctive mechanism to realize FFLO states by creating an imbalance in the quantum geometry of paired electrons on an isolated flat band, which we term “*Quantum Geometry Discrepancy* (QGD)”. Based on a flat-band electronic Hamiltonian with continuously tunable quantum metrics for each spin species, we analytically investigate the QGD-induced FFLO instability near the superconducting critical temperature through the band-projection method. To obtain the phase diagram of the BCS-FFLO transition driven by QGD, we perform numerical calculations using self-consistent mean-field theory, which aligns well with the analytical results. Additionally, we discuss the stability of the flat-band FFLO state when a finite band dispersion is turned on. We point out that QGD serves as a new protocol for stabilizing the FFLO states in flat-band superconductors.

*Introduction.*—The Fulde–Ferrell–Larkin–Ovchinnikov (FFLO) pairing state in superconductors is characterized by Cooper pairs with finite center-of-mass momentum  $\mathbf{Q}$ , originally proposed to be facilitated by the Zeeman effect of an external magnetic field [1–4]. Two typical FFLO pairing states with the spatially modulated order parameters include the Fulde–Ferrell (FF) type [1]  $e^{i\mathbf{Q}\cdot\mathbf{r}}$  and the Larkin–Ovchinnikov (LO) type [2]  $\cos(\mathbf{Q}\cdot\mathbf{r})$ . Although major attention has been focused on the interplay between the Zeeman effect and spin-orbital interaction [3, 5–8], it was investigated theoretically [9–13] and demonstrated experimentally [14] that the interlayer orbital effect from an in-plane magnetic field could assist FFLO formation in a multilayer Ising superconductor where the Zeeman effect is suppressed [15–18], which is referred as orbital FFLO state.

Existing mechanisms for FFLO states mentioned above have been investigated mainly concerning the Fermi surface mismatch. However, the quantum geometry, which dictates the structure of Bloch functions within a band [19], remains rarely explored in shaping FFLO states [20], especially in the context of flat-band superconductors. The recent experimental observations [21] in flat-band superconductors have revealed several non-trivial features that violate BCS theory for its vanishing Fermi velocity  $v_F$ . In flat-band superconductors, the wave-function quantum geometry defines the superfluid density [22–33] and coherence length [34, 35]. Several recent theoretical works have also studied the density wave instabilities related to quantum geometry, including the charge density wave [36] and pair density wave [37–41].

In this work, we unveil a new scheme for the FFLO states in flat-band superconductors induced by “*Quantum Geometry Discrepancy* (QGD)”, which refers to the difference in the wave-function quantum geometry be-

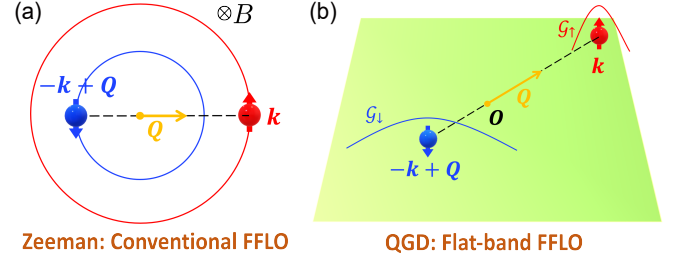


FIG. 1. Schematic illustrations of (a) conventional FFLO from Zeeman effect, and (b) flat-band FFLO from QGD. In (a), an external  $B$  field induces spin imbalance with finite momentum  $\mathbf{Q}$ , where  $|\mathbf{Q}| \propto B/v_F$ . In (b), the finite momentum  $\mathbf{Q}$  is stabilized when the quantum metrics of the paired electrons are different ( $\mathcal{G}_\uparrow \neq \mathcal{G}_\downarrow$ ) for flat-band superconductors.

tween the two electrons forming a Cooper pair. In the originally proposed FFLO state, the spin-singlet pairing state with finite center-of-mass momentum  $\mathbf{Q}$  ( $|\mathbf{Q}| \propto B/v_F$ ) is favorable [see Fig. 1(a)] in the presence of Zeeman field  $B$ . However, this microscopic mechanism breaks down in flat-band superconductors, due to the unphysical divergence of  $\mathbf{Q}$  when  $v_F \rightarrow 0$ , if a finite magnetic field is applied. In our proposal, we find that even as  $v_F \rightarrow 0$ , the finite momentum  $\mathbf{Q}$  can be stabilized when the pairing is frustrated by QGD, i.e.,  $\mathcal{G}_\uparrow \neq \mathcal{G}_\downarrow$  [see Fig. 1(b)]. Here  $\mathcal{G}_\uparrow$  and  $\mathcal{G}_\downarrow$  denote the quantum metric of the Bloch functions for paired electrons.

This work is organized as follows. First, we analyze the superconducting Gaussian fluctuations near the critical temperatures in the band-projection formalism regarding the superconductivity in a concrete flat-band model with a tunable quantum metric. We illustrate that QGD frustrates the singlet pairing by explicitly breaking the time-reversal ( $\mathcal{T}$ ) symmetry between the paired

electrons on their wave function, rather than band dispersion. As a consequence, the pairing susceptibility at non-zero  $\mathbf{q} = \mathbf{Q}$  can be larger than at  $\mathbf{q} = 0$  when a sizeable QGD exists, which leads to the FFLO state being more favorable. Then, as a comparison, we employ the self-consistent mean-field study for the FFLO state. This way, we obtain the phase diagram and identify the BCS-FFLO first-order phase transition points driven by QGD at different temperatures. This aligns well with the analytical results near the critical temperature. Besides, we find the region of QGD-stabilized FFLO states persisting even for a weakly dispersive band. Finally, we discuss some possible extensions to the present study.

*Model.*—We begin our analysis by defining a two-orbital, spinful tight-binding model with isolated flat bands and separate tunable quantum metric for each spin species, which is adapted from Ref. [36, 42, 43], and we term as “ $\zeta$ -lattice” [44]. In Fig. 2(a), the  $\zeta$ -lattice has  $A$  and  $B$  orbitals per site and the Hamiltonian can be written as  $H = \sum_{\mathbf{k}\sigma} \hat{c}_{\mathbf{k}\sigma}^\dagger \mathcal{H}_{\mathbf{k}\sigma} \hat{c}_{\mathbf{k}\sigma}$  with

$$\begin{aligned} \mathcal{H}_{\mathbf{k}\sigma} &= -t(\lambda_x \sin \alpha_{\mathbf{k},\sigma} + m_\sigma \lambda_y \cos \alpha_{\mathbf{k},\sigma}) - \mu_\sigma \lambda_0, \\ \alpha_{\mathbf{k},\sigma} &= \zeta_\sigma (\cos k_x a + \cos k_y a), \end{aligned} \quad (1)$$

where the fermion operators with spin  $\sigma = \uparrow, \downarrow$  are  $\hat{c}_{\mathbf{k}\sigma} = (\hat{c}_{A,\mathbf{k}\sigma}, \hat{c}_{B,\mathbf{k}\sigma})^T$ , and the periodic function  $\alpha_{\mathbf{k},\sigma}$  contains spin-dependent long range hoppings as depicted in Fig. 2(a). Here we set the lattice constant  $a = 1$  and  $\mu_\uparrow = \mu_\downarrow = \mu$  for brevity. The Pauli matrices  $\lambda_i$  act on orbital space, meanwhile  $m_{\sigma=\uparrow/\downarrow} = \pm 1$ . This model exhibits a pair of ideal isolated flat bands with band gap  $2t$  for each spin [the red solid lines in Fig. 2(b)], i.e.,  $\xi_{\mathbf{k}\sigma} = \pm t - \mu$  and the corresponding Bloch wave functions are  $u_{\mathbf{k}\sigma} = (\pm 1, im_\sigma e^{im_\sigma \alpha_{\mathbf{k}\sigma}})^T / \sqrt{2}$ .

In the  $\zeta$ -lattice model,  $\zeta_\sigma > 0$  characterizes the magnitude of the quantum metric  $\mathcal{G}_{\mathbf{k}\sigma}$  (proportional to  $\zeta_\sigma^2$  [36]) of the isolated flat band for spin- $\sigma$ . Note that when  $\zeta_\uparrow = \zeta_\downarrow$ , the model is  $\mathcal{T}$  symmetric [42], i.e.,  $u_{\mathbf{k}\uparrow} = u_{-\mathbf{k}\downarrow}^*$  and  $\mathcal{G}_{\mathbf{k}\uparrow} = \mathcal{G}_{\mathbf{k}\downarrow}$ . However, when  $\zeta_\uparrow \neq \zeta_\downarrow$ , the spin-up electron at  $\mathbf{k}$  and spin-down electron at  $-\mathbf{k}$  are still degenerate in energy, i.e.,  $\xi_{\mathbf{k}\uparrow} = \xi_{-\mathbf{k}\downarrow}$  but are polarized in quantum metric, i.e.,  $\mathcal{G}_{\mathbf{k}\uparrow} \neq \mathcal{G}_{\mathbf{k}\downarrow}$ . In this situation, the  $\mathcal{T}$  symmetry of the system is explicitly broken, which is manifested by  $u_{\mathbf{k}\uparrow} \neq u_{-\mathbf{k}\downarrow}^*$ , rather than the energy difference. We refer to this behavior as the QGD between the paired electrons  $[(\mathbf{k}, \uparrow)$  and  $(-\mathbf{k}, \downarrow)]$ . To capture it, we define a generalized quantum distance by  $d_{\mathbf{k},\mathbf{k}'}^2 = 1 - |\sum_\alpha u_{\mathbf{k}\uparrow}(\alpha) u_{\mathbf{k}'\downarrow}(\alpha)|^2$ . If the paired electrons are related by  $\mathcal{T}$  symmetry, their wavefunctions possess the shortest distance of  $d_{\mathbf{k},-\mathbf{k}} = 0$ . For the  $\zeta$ -lattice model, we utilize the dimensionless parameter  $\eta = |\zeta_\uparrow - \zeta_\downarrow| / (\zeta_\uparrow + \zeta_\downarrow)$  (we name it as “QGD degree”) as a global measurement of the QGD between the spin-up and spin-down sectors. For small  $\eta$ , we have  $d_{\mathbf{k},-\mathbf{k}} \propto \eta$ . In the following sections, we will demonstrate how the QGD induces the FFLO phase in flat-band superconduc-

tors.

*Effective action from band-projection method.*—To illustrate the essential role played by QGD in stabilizing the flat-band FFLO state, we analyze the static superconducting Gaussian fluctuations by employing the band-projection formalism [34, 40, 45, 46]. Without loss of generality, we consider the local Hubbard interaction  $\hat{\mathcal{H}}_I = -U \sum_{i\alpha} \hat{c}_{i\alpha\uparrow}^\dagger \hat{c}_{i\alpha\downarrow}^\dagger \hat{c}_{i\alpha\downarrow} \hat{c}_{i\alpha\uparrow}$ , where  $U > 0$  denotes attraction,  $\alpha$  and  $i$  denote the orbital and site index. Under the uniform pairing condition [32, 33] (which is accurate near the critical temperature in this model, as the numerical calculations suggest; for details, see Supplemental Material [47]), after the Fourier transformation ( $\hat{c}_{i\alpha\sigma} = 1/\sqrt{N_c} \sum_{\mathbf{k}} e^{i\mathbf{k}\cdot\mathbf{r}_i} \hat{c}_{\alpha,\mathbf{k}\sigma}$ , where  $N_c$  is the number of unit cells), we arrive at an effective interaction in the momentum space

$$\hat{\mathcal{H}}_I = -g \sum_{\alpha\beta\mathbf{k}\mathbf{k}'\mathbf{q}} \hat{c}_{\alpha,\mathbf{k}+\mathbf{q}\uparrow}^\dagger \hat{c}_{\alpha,-\mathbf{k}\downarrow}^\dagger \hat{c}_{\beta,-\mathbf{k}'\downarrow} \hat{c}_{\beta,\mathbf{k}'+\mathbf{q}\uparrow}, \quad (2)$$

with the coupling constant  $g = U/N_c N_{orb}$ , where  $N_{orb} = 2$  is the number of orbitals in each unit cell. We assume a weak interaction, i.e., the energy scale of the interaction is much smaller than the band gap ( $g \ll 2t$ ) such that the higher band has a minor impact.

To analyze the low-energy behaviors of the superconductivity that occurs on the relevant isolated flat band from field theory, we project the interaction onto the target flat band by  $\hat{c}_{\alpha,\mathbf{k}\sigma} \rightarrow u_{\mathbf{k}\sigma}^*(\alpha) \hat{a}_{\mathbf{k}\sigma}$ , where  $\hat{a}_{\mathbf{k}\sigma}$  denotes electron annihilation operator. We can obtain

$$\begin{aligned} \hat{\mathcal{H}}_I &\rightarrow -g \sum_{\mathbf{q}} \hat{\theta}_{\mathbf{q}}^\dagger \hat{\theta}_{\mathbf{q}}, \\ \hat{\theta}_{\mathbf{q}} &= \sum_{\mathbf{k}} \Lambda^*(\mathbf{k}, \mathbf{q}) \hat{a}_{-\mathbf{k}\downarrow} \hat{a}_{\mathbf{k}+\mathbf{q}\uparrow}, \end{aligned} \quad (3)$$

in which  $\Lambda(\mathbf{k}, \mathbf{q}) = \sum_\alpha u_{\mathbf{k}+\mathbf{q}\uparrow}(\alpha) u_{-\mathbf{k}\downarrow}(\alpha)$  is the form factor, which encodes the information of quantum geometry within the relevant band [34, 35].

After arriving at an effective one-band description in the functional integral formalism [48], we adopt the standard Hubbard-Stratonovich decoupling of Eq. (3) to derive the effective action  $S[\Delta_{\mathbf{q}}]$  (for details see Supplemental Material [47]) of the superconducting order parameter field  $\Delta_{\mathbf{q}}$  with four-momentum  $\mathbf{q} = (\mathbf{q}, \Omega_m)$  with  $\Omega_m$  being the bosonic Matsubara frequencies. By retaining the second order terms of  $\Delta_{\mathbf{q}}$  in  $S[\Delta_{\mathbf{q}}]$ , we get the Gaussian action around the trivial saddle point  $\Delta_{\mathbf{q}} = 0$  as

$$S_G[\Delta_{\mathbf{q}}] = \sum_{\mathbf{q}} \Gamma_{\mathbf{q}}^{-1} |\Delta_{\mathbf{q}}|^2, \quad (4)$$

where the coefficient  $\Gamma_{\mathbf{q}}^{-1} = g^{-1} - \chi_{\mathbf{q}}^c$  is the pairing propagator, and the static pairing correlation function  $\chi_{\mathbf{q}}^c \equiv \chi_{\mathbf{q}=(\mathbf{q},0)}^c$  reads

$$\chi_{\mathbf{q}}^c = \frac{1}{N_c} \sum_{\mathbf{k}} \frac{1 - n_F(\xi_{\mathbf{k}+\mathbf{q}}) - n_F(\xi_{\mathbf{k}})}{\xi_{\mathbf{k}+\mathbf{q}} + \xi_{\mathbf{k}}} |\Lambda(\mathbf{k}, \mathbf{q})|^2. \quad (5)$$

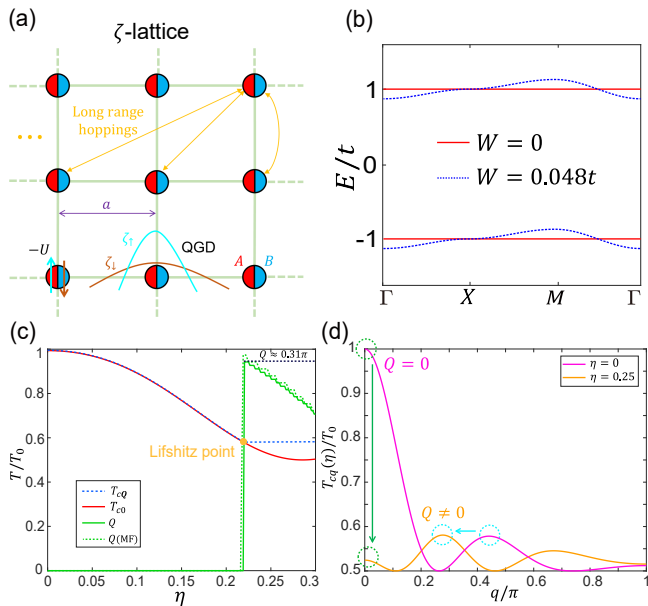


FIG. 2. (a) The  $\zeta$ -lattice with long-range hoppings and tunable quantum metric. (b) Band structure of (a), and the solid red (dashed blue) lines denote flat-band limit ( $W = 0$ ) and finite bandwidth ( $W = 0.048t$ ), respectively. (c)  $T_{c\mathbf{Q}}(\eta)$  (dashed blue),  $T_{c0}(\eta)$  (solid red), and the corresponding  $\mathbf{Q}(\eta)$  (solid green) from Eq. (6) as a function of  $\eta$ . The orange dot denotes the Lifshitz point. The  $\mathbf{Q}(\eta)$  calculated from the self-consistent mean-field (MF) theory is plotted in the dashed green line as a comparison. (d) Calculated  $T_{c\mathbf{q}}(\eta)/T_0$  from Eq. (6) on  $\mathbf{q} = q(\hat{x} + \hat{y})$ ,  $q \in [0, \pi]$ , for  $\eta = 0$  and  $\eta = 0.25$ , respectively. We set  $\zeta_{\downarrow} = 3$  and  $\zeta_{\uparrow} = \zeta_{\downarrow}(1 + \eta)/(1 - \eta)$ .

Here we have assumed  $\xi_{\mathbf{k}} = \xi_{\mathbf{k}\uparrow} = \xi_{-\mathbf{k}\downarrow}$  and  $n_F$  denotes the Fermi-Dirac distribution. The number equation near the critical temperature is  $N = -\beta^{-1} \partial S_G[\Delta_{\mathbf{q}} = 0] / \partial \mu$ , where  $N$  is the total particle number. We can obtain  $2\mathcal{A}\nu = \sum_{\mathbf{k}} [1 - \tanh(\beta\xi_{\mathbf{k}}/2)]$ , where  $\mathcal{A}$  is the area of the first Brillouin zone,  $\beta^{-1} = k_B T$ , and  $\nu$  is the filling factor of the target band ( $0 \leq \nu \leq 1$ ).

From the linearized gap equation  $g\chi_{\mathbf{q}}^c = 1$  together with the number equation, we can obtain the critical temperature  $T_{c\mathbf{q}}$  for the instability of a static spatially non-uniform pairing state with the finite  $\mathbf{q}$  index. Restricting the analysis to single- $\mathbf{q}$  states,  $\Delta_{\mathbf{q}} \propto \delta_{\mathbf{q}, \mathbf{Q}}$ , the value of  $\mathbf{Q}$  is found at highest  $T_{c\mathbf{q}}$ . If  $\mathbf{Q} \neq 0$  ( $\mathbf{Q} = 0$ ), this implies that the instability is associated with the FFLO (BCS) state with the finite (zero) momentum  $\mathbf{Q}$ .

Importantly, in the ideal flat-band limit, we find  $\chi_{\mathbf{q}}^c = \beta \sum_{\mathbf{k}} |\Lambda(\mathbf{k}, \mathbf{q})|^2 (1/2 - \nu) / [N_c \ln(\nu^{-1} - 1)]$ , thus  $T_{c\mathbf{q}}$  with fixed band filling and coupling constant, can be obtained as

$$T_{c\mathbf{q}}(\eta)/T_0 = 1 - d_{\eta}^2(\mathbf{q}), \quad (6)$$

in which the average of the generalized quantum distance is defined as  $d_{\eta}^2(\mathbf{q}) = \sum_{\mathbf{k}} d_{\mathbf{k}+\mathbf{q}, -\mathbf{k}}^2 / \mathcal{A}$ , and  $T_0 = T_{c\mathbf{q}=0}(\eta = 0)$ . When concerning the  $\zeta$ -lattice model,

both  $T_{c\mathbf{q}}$  and  $d_{\eta}^2(\mathbf{q})$  depend on  $\eta$ . The highest critical temperature at a fixed  $\eta$  should be determined by  $T_{c\mathbf{Q}}(\eta) = T_0 \{1 - \min[d_{\eta}^2(\mathbf{q})]\}$  over different  $\mathbf{q}$  in the first Brillouin zone, and the corresponding optimal momentum is  $\mathbf{q} = \mathbf{Q}(\eta)$ .

In terms of this method, in Fig. 2(c) we plot  $T_{c\mathbf{Q}}(\eta)$  (dashed blue) as well as the corresponding  $\mathbf{Q}(\eta)$  (solid green) from Eq. (6). As a comparison,  $T_{c0}(\eta)$  (solid red) is also plotted. In the BCS phase when  $\eta < \eta_c = 0.22$ ,  $T_{c\mathbf{Q}}(\eta)$  is identical to  $T_{c0}(\eta)$ , and  $\mathbf{Q}(\eta) = 0$ . However, when  $\eta > \eta_c$ ,  $T_{c\mathbf{Q}}(\eta) \neq T_{c0}(\eta)$ , and a sharp transition occurs in  $\mathbf{Q}(\eta)$  [from  $\mathbf{Q}(\eta_c^-) = 0$  to  $\mathbf{Q}(\eta_c^+) \approx 0.31\pi$ ], which implies a first-order transition from BCS to FFLO state. The tricritical point (orange dot) of BCS, FFLO, and the normal state is the so-called Lifshitz point, which is located at  $(\eta_c = 0.22, T = 0.57T_0)$ . In our calculations, we take  $\mathbf{Q} = Q(\hat{x} + \hat{y})$  throughout this work.

Since the highest critical temperature is determined by the minimum of  $d_{\eta}^2(\mathbf{q})$ , to understand the role of QGD in the BCS-FFLO transition, we examine  $T_{c\mathbf{q}}(\eta)/T_0$  from Eq. (6) in Fig. 2(d), for  $\eta = 0$  (pink curve) and  $\eta = 0.25$  (orange curve), respectively. When the  $\mathcal{T}$  symmetry is preserved ( $\eta = 0$ ), the BCS state is favored because  $\mathbf{Q} = 0$  is the global minimum of  $d_0^2(\mathbf{q})$ , namely  $d_0^2(\mathbf{q}) \geq d_0^2(0) = 0$  for any  $\mathbf{q}$ . This also corresponds to the global maximum of  $T_{c\mathbf{q}}(0)$  (dashed green circle on the pink curve). Note that local minima of  $d_0^2(\mathbf{q})$  are also found at nonzero  $\mathbf{q}$  [local maxima of  $T_{c\mathbf{q}}(0)$ , the dashed cyan circle on the pink curve]. As QGD ( $\eta \neq 0$ ) increases  $d_{\eta}^2(0)$  significantly [ $d_{\eta}^2(0) \propto \eta^2$  for small  $\eta$ ], and the  $T_{c0}(\eta)$  decreases dramatically (the green dashed circle on the orange curve), the value of  $d_{\eta}^2(\mathbf{q})$  at these local minima does not change much. With an increased  $\eta$ , these local minima finally transition to global minima (the cyan dashed circle on the orange curve) at  $\mathbf{Q}(\eta) \neq 0$ , where QGD drives the system to a FFLO state.

*Numerical study from self-consistent mean field theory.*—The pairing susceptibility analysis from the band projection method implies a wide range of QGD degree  $\eta$  for the FFLO instabilities. However, the uniform pairing condition may not apply when we consider low temperatures  $T \ll T_c$ . To remedy this problem, based on the self-consistent mean field theory [20], in this section, we numerically show the first-order phase transition from the BCS to the FFLO state driven by QGD for the  $\zeta$ -lattice model introduced previously. Here, we assume the single-harmonic FF-type ansatz, so the mean-field decoupling of the attractive Hubbard interaction yields the orbital-dependent order parameters  $\Delta_{\mathbf{r}\alpha} = -U \langle \hat{c}_{\mathbf{r}\alpha\downarrow} \hat{c}_{\mathbf{r}\alpha\uparrow} \rangle = \Delta_{\alpha}(\mathbf{q}) e^{i\mathbf{q}\cdot\mathbf{r}}$  with  $\mathbf{q}$  index. In the canonical ensemble, the Helmholtz free energy  $F$  says

$$F[\mu_{\mathbf{q}}, \Delta_{\alpha}(\mathbf{q}), \mathbf{q}] = \frac{1}{U} \sum_{\alpha} |\Delta_{\alpha}(\mathbf{q})|^2 - \frac{1}{\beta} \sum_{\mathbf{k}} \text{Tr} \left[ \ln \left( 1 + e^{-\beta H_{\text{BdG}}(\mathbf{k}, \mathbf{q})} \right) \right]. \quad (7)$$

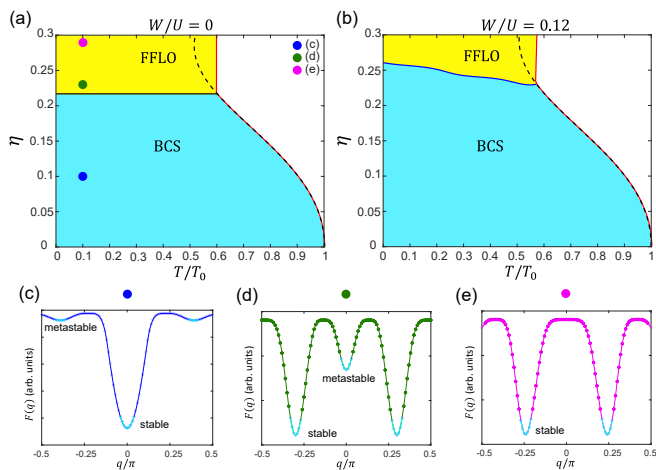


FIG. 3. The superconducting phase diagram of the  $\zeta$ -lattice model, without (a) and with (b) band dispersion. The dashed black line labels  $T_{c0}(\eta)$ , while the solid red line labels  $T_{c\mathbf{Q}}(\eta)$ . The BCS and FFLO phases are colored in light blue and yellow, respectively. Parameters used here:  $U = 0.4t$ ,  $\nu = 0.5$ ,  $\zeta_{\downarrow} = 3$ ,  $W/U = 0$  in (a) and  $W/U = 0.12$  in (b). (c) (d) (e): The free energy landscapes of three highlighted dots in (a) with  $T = 0.1T_0$  but different  $\eta$  ( $\eta = 0.10, 0.23$ , and  $0.29$ , respectively).

where the Bogoliubov–de Gennes (BdG) Hamiltonian  $H_{\text{BdG}}(\mathbf{k}, \mathbf{q})$  says

$$H_{\text{BdG}}(\mathbf{k}, \mathbf{q}) = \begin{pmatrix} \mathcal{H}_{\mathbf{k}+\mathbf{q}\uparrow} - \mu_{\mathbf{q}} & \hat{\Delta}_{\mathbf{q}} \\ \hat{\Delta}_{\mathbf{q}}^{\dagger} & -\mathcal{H}_{-\mathbf{k}\downarrow} + \mu_{\mathbf{q}} \end{pmatrix}, \quad (8)$$

with the order parameters  $\hat{\Delta}_{\mathbf{q}} = \text{diag}[\Delta_A(\mathbf{q}), \Delta_B(\mathbf{q})]$ .  $\hat{\Delta}_{\mathbf{q}}$  and  $\mu_{\mathbf{q}}$  are determined simultaneously by solving the gap and number equations, respectively. After substituting  $\hat{\Delta}_{\mathbf{q}}$  and  $\mu_{\mathbf{q}}$  into Eq. (7), we can obtain the minimized free energy  $F(\mathbf{q})$  for each  $\mathbf{q}$  (more details can be found in the Supplemental Material [47]).

The results from mean-field calculations are summarized in Fig. 3. As shown in Fig. 3(a), the BCS regime and the FFLO regime are colored light blue and yellow, respectively.  $T_{c0}(\eta)$  and  $T_{c\mathbf{Q}}(\eta)$  are plotted in the dashed black curve and the solid red curve. The most favored pairing momentum  $\mathbf{Q}(\eta)$  is independent of the temperature, so the phase boundary between the BCS and FFLO state is a straight line. The calculated  $T_{c0}(\eta)$ ,  $T_{c\mathbf{Q}}(\eta)$  and  $\mathbf{Q}(\eta)$  ( $\mathbf{Q}(\eta)$  are also plotted in Fig. 2(a) in a dashed green curve to compare with the one evaluated from the band projection method) exhibit quantitatively good agreements with the corresponding analytical results in Fig. 2(c). To provide a clear picture of the phase transition, in Fig. 3(c) to (e), we show the landscapes of free energy  $F(\mathbf{q})$  along the  $\mathbf{q} = q(\hat{x} + \hat{y})$  direction for the three points (dark blue, green, and pink dots) in Fig. 3(a). Initially, in the BCS region [Fig. 3(c)], the global minimum of the free energy  $F(\mathbf{q})$  is at  $\mathbf{q} = 0$ , which is stable under fluctuations. Some local minima exist at  $\mathbf{q} \neq 0$  but are

metastable. When  $\eta > \eta_c$  [Fig. 3(d)], now  $\mathbf{q} = 0$  turns into a local minimum but remains a metastable state, while some  $\mathbf{q} = \mathbf{Q}$  points become global minima (the model respects  $C_4$  rotational symmetry, so the minima have four-fold degeneracy in the whole Brillouin zone), the system enters the FFLO phase. This fact implies that the QGD energetically penalizes the BCS pairing more than the FFLO pairing, matching the picture we obtained from the band-projection method. As  $\eta$  continues to increase [Fig. 3(e)], finally, the local minimum at  $\mathbf{q} = 0$  loses its stability.

*Robustness at finite bandwidth.*—The QGD-induced BCS-FFLO phase transition has been examined in the ideal flat-band case, both analytically and numerically. To show the robustness of QGD-induced BCS-FFLO transition with finite band dispersion, we modify the model Hamiltonian as

$$\mathcal{H}_{\mathbf{k}\sigma} \rightarrow \mathcal{H}_{\mathbf{k}\sigma} - \frac{W}{4} (\cos k_x a + \cos k_y a) \lambda_0, \quad (9)$$

where an additional nearest hopping term brings a finite bandwidth  $W$  as shown in Fig. 2(b). In this case, the Bloch wave functions remain unchanged. We keep  $W \ll U$  to ensure a narrow bandwidth compared to the interaction. In Fig. 3(b), the calculated phase diagram at  $W/U = 0.12$  ( $U = 0.4t$ ) is shown. It is clear that the transition boundary line gets curved due to the nonzero  $W$ , and requires a larger QGD to reach the FFLO region compared with Fig. 3(a), especially at lower temperatures. These results implies that at finite  $W$ , higher  $T$  is needed to enter the FFLO phase because the thermal energy  $k_B T$  overcomes the effect from finite bandwidth. In this scenario,  $k_B T$  is close to the interaction, i.e.,  $k_B T \sim U$ , resulting in prominent effect from QGD. On the other hand, for conventional superconductors we have  $W \gg U \gg k_B T$  in the weak coupling regime, where the QGD-driving mechanism for the FFLO state may not work (more discussions, see Supplemental Material [47]).

*Conclusion and Discussion.*—In this work, we have identified a quantum-geometric origin of the FFLO state, called QGD, particularly in flat-band superconductors. QGD explicitly breaks  $\mathcal{T}$  symmetry by creating a mismatch in the quantum geometry of paired electrons. This mechanism differs from other pair-breaking mechanisms, which produce energy (population) imbalances between paired electrons, such as the Zeeman effect or the orbital effect of an in-plane magnetic field in layered superconductors. Here we only consider the QGD-stabilised FFLO state for the  $s$ -wave pairing channel. But there is no obstacle in generalizing it to other pseudo-spin degrees of freedom (such as valley and layer) and unconventional pairing channels.

Besides, in this work we expect the LO-type pairing state to be more stable than the FF type because the  $\pm\mathbf{Q}$  states are degenerate in energy for the inversion-symmetric model Hamiltonian in Eq. (1). By turning

on an extra inversion-breaking term in the Bloch wave functions of the model, the  $\pm Q$  degeneracy is lifted, resulting in the FF type pairing state and superconducting diode effect (for more details, see Supplemental Material [47]). This is an analog to the helical superconductors with Rashba spin-orbit interaction and in-plane magnetic fields [3, 8].

One possible route to a realistic model with QGD in solid-state systems is through light-matter interaction. Recently, chiral optical cavities have been proposed to induce  $\mathcal{T}$  symmetry breaking in quantum materials [49, 50], reshaping the topology and quantum geometry of the electronic states [50]. An explicit scheme of QGD through cavity engineering remains a topic for future study. Another option is in ultracold atom systems, where neutral superfluidity can be achieved in low-dimensional optical lattices. In this scenario, a state-dependent optical lattice with spin-dependent hopping parameters [3, 51], which has been previously used to introduce effective mass imbalance, could potentially mimic the effect of QGD.

*Acknowledgements*—We thank Xiao-Gang Wen, Xilin Feng, Ying-Ming Xie, Akito Daido, and Qing-Dong Jiang for inspiring discussions. K. T. L. acknowledges the support of the Ministry of Science and Technology, China, and Hong Kong Research Grant Council through Grants No. 2020YFA0309600, No. RFS2021-6S03, No. C6025-19G, No. AoE/P-701/20, No. 16310520, No. 16307622, and No. 16309223.

---

\* These authors contributed equally to this work.

† jinxin.hu@ntu.edu.sg

‡ phlaw@ust.hk

- [1] P. Fulde and R. A. Ferrell, *Physical Review* **135**, A550 (1964).
- [2] A. Larkin and Y. N. Ovchinnikov, *Soviet Physics-JETP* **20**, 762 (1965).
- [3] J. J. Kinnunen, J. E. Baarsma, J.-P. Martikainen, and P. Törmä, *Reports on Progress in Physics* **81**, 046401 (2018).
- [4] D. F. Agterberg, J. S. Davis, S. D. Edkins, E. Fradkin, D. J. Van Harlingen, S. A. Kivelson, P. A. Lee, L. Radzihovsky, J. M. Tranquada, and Y. Wang, *Annual Review of Condensed Matter Physics* **11**, 231 (2020).
- [5] V. Barzykin and L. P. Gor'kov, *Physical review letters* **89**, 227002 (2002).
- [6] Z. Zheng, M. Gong, Y. Zhang, X. Zou, C. Zhang, and G. Guo, *Scientific reports* **4**, 6535 (2014).
- [7] M. Sigrist, D. F. Agterberg, M. H. Fischer, J. Goryo, F. Loder, S.-H. Rhim, D. Maruyama, Y. Yanase, T. Yoshida, and S. J. Youn, *Journal of the Physical Society of Japan* **83**, 061014 (2014).
- [8] M. Smidman, M. Salamon, H. Yuan, and D. Agterberg, *Reports on Progress in Physics* **80**, 036501 (2017).
- [9] C.-X. Liu, *Physical Review Letters* **118**, 087001 (2017).
- [10] K. W. Song and A. E. Koshelev, *Physical Review X* **9**, 021025 (2019).
- [11] Y.-M. Xie and K. Law, *Physical Review Letters* **131**, 016001 (2023).
- [12] N. F. Q. Yuan, *Phys. Rev. Res.* **5**, 043122 (2023).
- [13] K. Nakamura, A. Daido, and Y. Yanase, *Physical Review B* **109**, 094501 (2024).
- [14] P. Wan, O. Zheliuk, N. F. Yuan, X. Peng, L. Zhang, M. Liang, U. Zeitler, S. Wiedmann, N. E. Hussey, T. T. Palstra, *et al.*, *Nature*, 1 (2023).
- [15] J. Lu, O. Zheliuk, I. Leermakers, N. F. Yuan, U. Zeitler, K. T. Law, and J. Ye, *Science* **350**, 1353 (2015).
- [16] X. Xi, Z. Wang, W. Zhao, J.-H. Park, K. T. Law, H. Berger, L. Forró, J. Shan, and K. F. Mak, *Nature Physics* **12**, 139 (2016).
- [17] B. T. Zhou, N. F. Yuan, H.-L. Jiang, and K. T. Law, *Physical Review B* **93**, 180501 (2016).
- [18] Y. Saito, Y. Nakamura, M. S. Bahramy, Y. Kohama, J. Ye, Y. Kasahara, Y. Nakagawa, M. Onga, M. Tokunaga, T. Nojima, *et al.*, *Nature Physics* **12**, 144 (2016).
- [19] P. Törmä, *Physical Review Letters* **131**, 240001 (2023).
- [20] T. Kitamura, A. Daido, and Y. Yanase, *Physical Review B* **106**, 184507 (2022).
- [21] H. Tian, X. Gao, Y. Zhang, S. Che, T. Xu, P. Cheung, K. Watanabe, T. Taniguchi, M. Randeria, F. Zhang, *et al.*, *Nature* **614**, 440 (2023).
- [22] S. Peotta and P. Törmä, *Nature communications* **6**, 8944 (2015).
- [23] A. Julku, S. Peotta, T. I. Vanhala, D.-H. Kim, and P. Törmä, *Physical Review Letters* **117**, 045303 (2016).
- [24] L. Liang, T. I. Vanhala, S. Peotta, T. Siro, A. Harju, and P. Törmä, *Physical Review B* **95**, 024515 (2017).
- [25] X. Hu, T. Hyart, D. I. Pikulin, and E. Rossi, *Physical Review Letters* **123**, 237002 (2019).
- [26] A. Julku, T. J. Peltonen, L. Liang, T. T. Heikkilä, and P. Törmä, *Physical Review B* **101**, 060505 (2020).
- [27] F. Xie, Z. Song, B. Lian, and B. A. Bernevig, *Physical review letters* **124**, 167002 (2020).
- [28] V. Peri, Z.-D. Song, B. A. Bernevig, and S. D. Huber, *Physical review letters* **126**, 027002 (2021).
- [29] P. He, H.-T. Ding, and S.-L. Zhu, *Physical Review A* **103**, 043329 (2021).
- [30] J. Herzog-Arbeitman, V. Peri, F. Schindler, S. D. Huber, and B. A. Bernevig, *Physical review letters* **128**, 087002 (2022).
- [31] P. Törmä, S. Peotta, and B. A. Bernevig, *Nature Reviews Physics* **4**, 528 (2022).
- [32] P. Törmä, L. Liang, and S. Peotta, *Physical Review B* **98**, 220511 (2018).
- [33] K.-E. Huhtinen, J. Herzog-Arbeitman, A. Chew, B. A. Bernevig, and P. Törmä, *Physical Review B* **106**, 014518 (2022).
- [34] S. A. Chen and K. T. Law, *Phys. Rev. Lett.* **132**, 026002 (2024).
- [35] J.-X. Hu, S. A. Chen, and K. T. Law, *arXiv preprint arXiv:2308.05686* (2023).
- [36] J. S. Hofmann, E. Berg, and D. Chowdhury, *Physical Review Letters* **130**, 226001 (2023).
- [37] G. Jiang and Y. Barlas, *Physical Review Letters* **131**, 016002 (2023).
- [38] W. Chen and W. Huang, *Science China Physics, Mechanics & Astronomy* **66**, 287212 (2023).
- [39] Z. Han, J. Herzog-Arbeitman, B. A. Bernevig, and S. A. Kivelson, *arXiv preprint arXiv:2401.04163* (2024).
- [40] N. S. Ticea, S. Raghu, and Y.-M. Wu, *arXiv preprint*

- arXiv:2403.00156 (2024).
- [41] H.-X. Wang and W. Huang, arXiv preprint arXiv:2406.17187 (2024).
- [42] J. S. Hofmann, D. Chowdhury, S. A. Kivelson, and E. Berg, npj Quantum Materials **7**, 83 (2022).
- [43] D. Mao and D. Chowdhury, Proceedings of the National Academy of Sciences **120**, e2217816120 (2023).
- [44] M. Thumin and G. Bouzerar, arXiv e-prints , arXiv (2024).
- [45] C. Setty, L. Fanfarillo, and P. Hirschfeld, Nature Communications **14**, 3181 (2023).
- [46] M. Iskin, Physical Review B **107**, 224505 (2023).
- [47] The Supplemental material of "Quantum Geometry Discrepancy Induced Flat-band FFLO State". Including three parts, I. Details of the self-consistent mean-field theory, II. Derivation of the Gaussian fluctuation in the band projection formalism, III. Some supplemental calculations.
- [48] A. Altland and B. Simons, *Condensed Matter Field Theory*, 3rd ed. (Cambridge University Press, 2023).
- [49] H. Hübener, U. De Giovannini, C. Schäfer, J. Andberger, M. Ruggenthaler, J. Faist, and A. Rubio, Nature materials **20**, 438 (2021).
- [50] F. Schlwin, D. M. Kennes, and M. A. Sentef, Applied Physics Reviews **9** (2022).
- [51] G. Jotzu, M. Messer, F. Görg, D. Greif, R. Desbuquois, and T. Esslinger, Physical review letters **115**, 073002 (2015).